Gemini surfactant assisted synthesis of mesoporous Mn/Mg bimetal doped TiO_2 nanomaterial: Characterization and photocatalytic activity studies under visible light irradiation

Sankara Rao Miditana
Andhra University
Siva Rao Tirukkovalluri (sivaraoau@gmail.com)
Andhra University https://orcid.org/0000-0001-5156-1885
Imandi Manga Raju
Andhra University
Shaik Abdul Alim
Andhra University
Genji Jaishree
Andhra University
M.L.V. Prasanna Chippada
Andhra University

Research

Keywords: Mn2+/Mg2+ bimetal doped TiO2, Gemini surfactant, Methyl Red, Mesoporous Nanocatalyst, Sol-gel technique, Anatase TiO2

Posted Date: January 25th, 2021

DOI: https://doi.org/10.21203/rs.3.rs-45648/v4

Version of Record: A version of this preprint was published at Sustainable Environment Research on February 10th, 2021. See the published version at https://doi.org/10.1186/s42834-021-00078-8.

Abstract

The present work mainly aimed to synthesize different weight percentages (0.25-1.00 wt%) of Manganese (Mn^{2+}) and Magnesium (Mg^{2+}) bimetal ions doped TiO_2 nanomaterial assisted with different weight percentages (5-15 wt%) of Gemini surfactant (GS) using sol-gel method. The bimetal doped and undoped TiO_2 photocatalysts were characterized by X-ray Diffraction, Scanning Electron Microscopy, Energy Dispersive X-ray Spectroscopy, Fourier Transform Infrared Spectroscopy (FT-IR), UV-Visible Diffused Reflectance Spectroscopy, Transmission Electron Microscopy, Brunauer-Emmett-Teller surface area analyzer, and Photoluminescence Spectroscopy. Characterization results revealed that mesoporous multi-particle anatase TiO_2 nanoparticles with a narrowed band gap, small particle size, and high surface area were formed due to the combined effect of Mn^{2+}/Mg^{2+} bimetal ions doping and effective encapsulation of GS over the initially formed TiO_2 nanoparticles. The surface elemental composition of the 0.25 wt% Mn^{2+} and 1.00 wt% Mg^{2+} bimetal doped TiO_2 in the presence of 10 wt% of GS (after calcination) revealed the presence of both the metal dopants Mn^{2+} and Mg^{2+} along with the Ti and O and their chemical interactions were further confirmed by FT-IR results. The photocatalytic activity of these catalysts was assessed by the degradation of Methyl Red using visible light irradiation. To understand the effect of different reaction parameters on the photocatalytic activity of the nanocatalysts such as the dopant concentration, surfactant concentration, catalyst dosage, solution pH, and initial dye concentrations were investigated and optimized to achieve the best performance. The photoluminescence results conclude that OH radicals are the crucial reactive species responsible for oxidative photocatalytic degradation of Methyl Red.

1. Introduction

It is worth noting that among the different semiconductors that are being studied from the past few decades for the photocatalytic degradation of various organic pollutants from wastewater, TiO_2 stands as the most preferable one due to its non-toxicity, non-corrosive, photostability, and low cost. To make it suitable for visible light activity, many attempts are being made to modify the TiO_2 electronic structure to overcome its disadvantages of high bandgap energy and high rate of electron-hole recombination. The recent literature findings revealed that bimetal ions doping into TiO_2 crystal lattice had overcome the above drawbacks and significantly enhanced its visible light activity [1-3]. Among the various metal ion dopants studied so far, transition metal ion dopants can greatly reduce the bad gap and electron-hole recombination by forming an extra energy level below the conduction band of TiO_2 due to the interaction of their 3d or 4d states with Ti 3d states [4]. Recently, Divya Lakshmi et al. [5] reported that Manganese (Mn^{2+}) is most preferable among the transition metals owing to the presence of t_2g orbital of d is very close to the conduction band of TiO_2 by which the absorption can be possibly shifted to the visible part of the spectrum. On the other hand, others [6-8] investigated the effect of Magnesium (Mg^{2+}), an alkaline earth metal, on the crystalline structure and catalytic activity of TiO_2 and found its absorption band was shifted more towards the visible region, which resulted in performing a high photocatalytic activity.

Hence, Mn^{2+} and Mg^{2+} ions could be more effective as metal ion dopants to modify the TiO_2 for better photocatalytic performance under visible light irradiation.

As the size, shape, and surface area of the photocatalyst play a major role in the photocatalytic degradation process of organic pollutants from wastewater, surfactants were the best-reported species to control the growth and agglomeration of nanoparticles during the synthesis process. Among those surfactants, more surface-active anionic Gemini surfactant, 1,4-Butane sultone (GS) plays an important role in effective encapsulation of initially formed TiO_2 particles to synthesize the spherical shaped bimetal doped TiO_2 nanoparticles with small grain size and large surface area [9]. Hence, in the present study, we aimed to synthesize the Mn^{2+} and Mg^{2+} bimetal doped TiO_2 nanoparticles in the presence of GS using the sol-gel process through which we can achieve high purity and homogeneous materials at room temperatures under stoichiometry control [10].

Compared to bulk materials, nanomaterials possess unique physical, chemical, and mechanical properties. To understand overall properties, it is important to characterize the structural, optical, and morphological properties of nanomaterials prior to proceed for different applications to obtain better results [11]. Hence, several advanced sophisticated techniques were used in the present study to characterize the crystalline phase, surface morphology, elemental composition, visible light absorption capacity, particle size, and surface area of as-synthesized bimetal doped TiO_2 nanoparticles to understand its suitability for photocatalytic degradation applications.

Due to the widespread industrial activities, various organic dye pollutants are being discharged into water bodies causing severe water pollution. Almost, 15% of the dyes produced worldwide are lost during synthesis and processing with wastewater. Moreover, 50% of all the dyes used in various industries are carcinogenic azo dyes, which are characterized by one or more azo bonds (-N=N-) [12] among which, Methyl Red (MR) is a familiar azo dye and is widely used in paper printing, textile dyeing, and leather industries [13]. It causes skin and eye irritation, irritation of the respiratory and digestive tract and is a suspected carcinogen, mutagen, and mitotic poison [14].

Hence, the removal of these pollutants from wastewaters in an eco-friendly way stands as a present major research concern. Therefore, in the present study, we attempted to remove this model azo dye pollutant from the contaminated water using as-synthesized Mn^{2+}/Mg^{2+} bimetal doped TiO_2 nanocatalysts, and their photocatalytic efficiency was tested by optimizing the important reaction parameters like dopant concentration, surfactant concentration, solution pH, catalyst dosage and initial dye concentration for the better water pollution abatement.

2. Experimental

2.1. Materials

All the chemicals used in this research were of reagent grade and used without any further purification. Titanium tetra-n-butoxide ($Ti(OBu)_4$), Manganese nitrate $[Mn(NO_3)_2]\cdot 6H_2O$, and Magnesium nitrate $[Mg(NO_3)_2]\cdot 6H_2O$ purchased from E-Merck Germany were used as precursors of TiO_2, Mn and Mg respectively, for preparing Mn^{2+}/Mg^{2+} bimetal doped TiO_2 samples. For the surfactant-assisted bimetal doped TiO_2 catalysts, GS obtained from Sigma Aldrich (Germany) was used. MR (High media, India.) was used as a model azo dye pollutant for photocatalytic degradation studies. Milli-Q water was used for the preparation of all the solutions.

2.2. Synthesis of nanocatalyst

Mn^{2+}/Mg^{2+} bimetal ions doped nanotitania and GS assisted Mn^{2+}/Mg^{2+} bimetal doped TiO_2 samples were prepared by sol-gel method. In this method, $Ti(OBu)_4$ (10 mL) was added to ethanol (20 mL) and acidified with 1.4 mL of HNO_3 taken in a pyrex glass vessel (Solution-I) and stirred for 20 min. Desired wt% (0.25-1.0 wt%) of Mn^{2+} and Mg^{2+} dopants proportionate to TiO_2 weight were taken in ethanol (20 mL) in another beaker and added 4.5 mL of Milli-Q water for effective hydrolysis purpose (Solution-II). Then the solution-II was slowly added to solution-I dropwise with continuous stirring. A colloidal solution that formed after complete mixing is further stirred for 90 min and aged for 48 h to obtain the gel. The formed gel was dried (at 70 °C), ground, and calcined at 450 °C for about 5 h in a furnace. To get homogeneous powder the calcined samples were well ground after cooling.

To optimize the best dopant concentrations, the photocatalytic efficiency of the as-synthesized bimetal doped TiO_2 samples was tested by degrading MR dye and 0.25 wt% Mn^{2+} and 1.00 wt% Mg^{2+} bimetal doped TiO_2 (MMT5) was found to be the best. For further enhancement in the photocatalytic activity of the MMT5 catalyst, GS assisted MMT5 nanocatalysts were synthesized by following the same procedure but different wt% (5, 10, and 15 wt%) of GS was added after the mixing of solution-I and solution-II. To study and compare the effect of dopants and surfactant on the photocatalytic properties of bimetal doped TiO_2, an undoped TiO_2 sample was prepared using the same procedure without adding dopants and surfactant precursors. Details and nomenclature of all the synthesized catalysts are presented in Table 1.

Table 1 Name assigned to different TiO_2 nanocatalyst samples

Serial number	Weight percentages of dopants (wt%)	Gemini surfactant wt%	Name given to the sample
1	0.25 Mn 0.75 Mg	-	MMT1
2	0.75 Mn 0.25 Mg	-	MMT2
3	0.50 Mn 0.50 Mg	-	MMT3
4	1.00 Mn 0.25 Mg	-	MMT4
5	0.25 Mn 1.00 Mg	-	MMT5
6	0.25 Mn 1.00 Mg	5	MMT5-GS1
7	0.25 Mn 1.00 Mg	10	MMT5-GS2
8	0.25 Mn 1.00 Mg	15	MMT5-GS3
9	NIL	-	Undoped TiO_2

2.3. Characterization techniques

The crystalline structure of photocatalysts was studied by powder X-ray diffraction (XRD) spectra using PANanalytical diffractometer with CuKα radiation (λ = 0.15405 nm) operated at 45 kV, 40 mA, and 0.2q min^{-1} scan rate. Based on the Scherrer equation using full width at half maximum (FWHM), the crystallite size of TiO_2 nanocatalysts was determined. The UV-Visible Diffuse reflectance spectra (UV-Vis DRS) of the catalysts were recorded in the range of 200-800 nm with a Shimadzu 3600 UV-Vis DRS Spectrophotometer using $BaSO_4$ as reference. Scanning electron microscopy (SEM) JSM 6300, Japan equipped with energy dispersive X-Ray (EDX) spectroscopy was used to investigate the surface morphology and elemental analysis, respectively. The microstructure and particle size of the samples were analyzed by high-resolution transmission electron microscopy (HRTEM) JEM-2100 JEOL at an operating voltage of 200 kV. Fourier transform infrared spectra (FT-IR) of the nanocatalysts were recorded on an FT-IR spectrometer (Nicolet Avatar360). Brunauer- Emmet-Teller (BET) surface area, pore size, and pore volume of the nanocatalysts were determined using Quanta Chrome Nova 2200E system by recording N_2 adsorption-desorption isotherms at 77.3 k. Photoluminescence (PL) analysis was performed by Hitachi F-7000 fluorescence spectrophotometer. The pH of the reaction mixture and the amount of MR degraded during the photocatalytic process were adjusted and monitored using Elico Digital pH meter (Model IIIE, EI) and UV-vis spectrophotometer (Shimadzu 1601), respectively.

2.4. Experimental procedure for the determination of visible light photocatalytic activity of nanocatalyst

The photocatalytic activity of surfactant-assisted Mn^{2+}/Mg^{2+} bimetal ions doped TiO_2 nanocatalyst was examined by the degradation of a model azo dye pollutant, MR in a visible light photoreactor as shown in Fig. 1. For visible light illumination, a high-pressure metal halide lamp (400 W, 35,000 lm, and 436-546 nm output) was used and placed 20 cm away from the pyrex glass vessel containing 100 mL of MR dye solution of desired concentration (1-10 mg L^{-1}) with sufficient amount of the catalyst. To screen the infrared radiation effect and to keep the constant temperature (25 °C) during the degradation experiments, water was passed continuously around the reaction vessel. Prior to visible light irradiation, the pH of the reaction mixture was adjusted to the desired value by the addition of 0.1 N NaOH/0.1 N HCl and the reaction mixture was stirred in dark for 30 min to establish the adsorption-desorption equilibrium between MR dye and surface of the catalyst [15]. After the visible light irradiation, 5 mL aliquots of samples were collected at regular time intervals using a Millipore syringe (0.45 μm) and change in the concentration of MR dye during the degradation process was studied with a UV-Vis spectrophotometer (Shimadzu 1601) by measuring its absorbance at 525 nm. The percentage degradation of MR was determined by using the Eq. (1) [16].

$$\%\ \text{degradation of MR} = \frac{C_0 - C_t}{C_0} \times 100 \qquad (1)$$

Where C_0 is the initial concentration of MR dye solution before degradation and C_t is the concentration at time t. For better photocatalytic degradation, the effect of reaction parameters like dopant concentration, surfactant concentration, solution pH, catalyst dosage, and initial dye concentration was studied and optimized by varying the measured parameter while keeping other parameters constant and the results are discussed in section 4.1-4.5. As the photocatalytic degradation of organic pollutants is mainly initiated by highly oxidative hydroxyl radicals (•OH), which can be easily captured by fluorescent probe molecules, the formation of •OH in the photocatalysis process was studied by PL technique using coumarin as a probe molecule [16].

3. Results And Discussion

3.1. XRD study

From the XRD patterns of all the synthesized catalysts shown in Fig. 2. All samples including undoped TiO_2 calcined at 450 °C for 5 h showed the formation of anatase phase having characteristic high-intensity diffraction peak at 2θ = 25.3° along with other corresponding small diffraction peaks at 2θ values 37.9, 48.1 and 54.1° that can be indexed to planes of (101), (004), (200) and (211) of anatase phase respectively (JCPDS No. 21-1272). No extra peak found at 2θ = 27.8°, indicating that there is no formation of the rutile phase. As the ionic radii of Mn^{2+} (0.78Å) and Mg^{2+} (0.72Å) are closer to the ionic radii of Ti^{4+} (0.68 Å), Mn^{2+} and Mg^{2+} dopant metal ions were expected to substitute Ti^{4+} ions in TiO_2 matrix which is confirmed by the absence of any diffraction peaks related to Mn and Mg oxides or other compounds [17, 18]. And it is also known that as the Mn^{2+} and Mg^{2+} are more electropositive, the electronic cloud in each TiO_2 might be loosely held, favoring the formation of less dense anatase phase [19]. The average crystallite sizes of the undoped, bimetal-doped (MMT) and surfactant-assisted bimetal doped (MMT-GS) catalysts were calculated based on the FWHM of the characteristic high intensified peak using Scherrer equation [1] ($d = k\lambda/\beta \cos\theta$), where d is the average crystallite size, k is 0.9 (Scherrer constant), λ is 1.5406 Å (X-ray wavelength), β is the FWHM and θ is the diffraction angle and are tabulated in Table 2. From the table, the average crystallite size of the catalysts was found to be ranging from 7.21-10.22, 10.86-12.87, and 18.30 nm for MMT-GS, MMT, and undoped TiO_2 nanocatalysts, respectively. The substitutional doping of metal ions into the TiO_2 lattice inhibited the grain growth by formation of Ti-O-Mn and Ti-O-Mg due to which the crystallite size was decreased in MMT catalysts. Further decrease in crystallite size was observed for the catalyst prepared in presence of surfactant, MMT-GS, which can be attributed to the effective capping nature of the GS which controls the nucleation and minimizes the agglomeration of TiO_2 nanoparticles during the synthesis process [20].

3.2. UV-Vis DRS study

From the UV-Vis DRS of the undoped TiO_2, MMT, and MMT-GS nanomaterials shown in Fig. 3a, it is observed that absorbance bands are shifted more towards the higher wavelengths, i.e., red-shifted in MMT and MMT-GS catalysts compared to undoped TiO_2, which is possibly due to the decreased bandgap

by co-doping of Mn^{2+} and Mg^{2+} into the TiO_2 matrix. The decrease in bandgap can be ascribed to the joint effect of these two metal dopant ions (Mn^{2+} and Mg^{2+}) in MMT and MMT-GS system, where these formed the extra energy levels below the conduction band of TiO_2 and thus reduces the electron-hole recombination by trapping electrons and enhances the visible light absorbance. From Fig. 3b it is further confirmed by bandgap energies obtained for all the synthesized catalysts using Kubelka-Monk formalism and Tauc plot method [21]. The corresponding band gap energy values are presented in Table 2. From the table, it is found that the average band gap values of the photocatalysts are in the range of 2.66-2.83, 2.68-2.97, and 3.20 eV for MMT-GS, MMT, and undoped TiO_2, respectively. These outcomes revealed that all MMT and MMT-GS catalysts are visible light active and can be used as better photocatalysts. The catalysts MMT5, MMT5-GS1, MMT5-GS2, and MMT5-GS3 have the same weight percentage of Mn and Mg; consequently, they have the absorption peaks nearly at the same wavelength. In particular, among all the MMT and MMT-GS catalysts, MMT5-GS2 showed the least bandgap energy, i.e., 2.66 eV.

Before proceeding to further characterization, we have conducted trial photocatalytic degradation experiments for all the synthesized catalysts using MR dye. From the results, it was noticed that among all the MMT catalysts, MMT5 exhibited better photocatalytic activity and moreover, MMT5 assisted with 10 wt% of GS, MMT5-GS2 has shown some more enhanced photocatalytic activity. Hence, we selected these two particular catalysts for further characterization with SEM-EDX, TEM, BET, FT-IR, and PL study.

3.3. SEM and EDX study

The SEM images shown in Fig. 4 illustrate the surface morphology of undoped TiO_2, MMT5, and MMT5-GS2, respectively. In comparison, it can be clearly seen that the morphology of the TiO_2 has been changed from large aggregates with a scratchy surface in undoped TiO_2 (Fig. 4a) to multiparticle agglomerated irregular shaped particles with rough surface in MMT5 (Fig. 4b) and pseudospherical less agglomerated nanoparticles with smooth surface area and small particle size in MMT-GS2 (Fig. 4c). This is clearly indicating that Mn^{2+} and Mg^{2+} bimetal ions doping and capping action with the GS have a significant impact on the morphology of TiO_2 nanoparticles which controls the grain growth and particle nucleation.

Also, the chemical composition of MMT5-GS2 sample was investigated by EDX with the results depicted in Fig. 5. Along with the Ti and O elements of TiO_2, the dopant elements Mn and Mg are found in the spectra supporting the presence of dopants in the TiO_2 matrix and there are no GS associated peaks are found in the spectra indicating complete elimination of GS after the calcination process. The quantitative analysis results are listed in a table inserted in Fig. 5 describing weight percentage as well as the atomic percentage of the compositional elements of the sample which indicates good compatibility with the dopant concentration used for the synthesis of TiO_2 nanoparticles.

3.4. TEM study

The TEM images of MMT5 and MMT5-GS2 photocatalysts are shown in Fig. 6a and b respectively. The TEM image (Fig. 6a) of MMT-5 shows pseudospherical shaped with multiparticle agglomeration and an average particle size of 6.6 nm. Whereas in MMT5-GS2 (Fig. 6b), most of the TiO_2 particles are well dispersed with very low agglomeration compare to Fig. 6a and the particle size is in the range of 2.3-5.4 nm, with an average particle size of 3.8 nm. Thus, it clearly indicates that the GS effectively inhibited the particle overgrowth and aggregation and resulted in small particle size with increased surface area, which is well correlated with BET results given in Table 2. The selected area electron diffraction (SAED) patterns shown in Fig. 6c confirmed the anatase phase with good crystallinity indexed by the concentric rings, which is in good agreement with XRD diffraction patterns. In addition to SAED, from the HRTEM image of MMT5-GS2 (Fig. 6d) the observed lattice fringes with d-spacing of 0.352 nm correspond to (101) plane of anatase and further confirms the single-crystal nature and high crystallinity of anatase TiO_2 [22].

3.5. FT-IR study

The incorporation of metal ion dopants, Mn^{2+} and Mg^{2+} into TiO_2 lattice was further confirmed by FT-IR results. The FT-IR spectra of the undoped TiO_2, MMT5, and MMT5-GS2 (before and after calcination) are shown in Fig. 7. The peaks at 3403.0, 2926.1, 1616.4, 1383.8, 3378.1, 2918.7, 1626.7, and 1372.1 cm^{-1} correspond to stretching vibrations of surface O-H and 3351.8, 2918.7, 1619.4 and 1383.8 cm^{-1} correspond to bending vibrations of adsorbed H_2O molecules [23]. The stretching vibrations of Ti-O and bending vibrations of Ti-O-Ti observed at 575.4 and 1375.8 cm^{-1} in undoped TiO_2 (Fig. 7a) were deformed/shifted to 620.3 and 1300.1 cm^{-1} in MMT5 (Fig. 7b) and 540.0 and 1182.0 cm^{-1} in MMT5-GS2 (Fig. 7c and d), respectively, which can be attributed to the presence of dopants in TiO_2 lattice. Hence, the FT-IR study confirms that Mn^{2+} and Mg^{2+} are substitutionally doped into TiO_2 lattice by replacing Ti^{4+} and formed a new network, i.e., Ti-O-Mn and Ti-O-Mg which are in good agreement with the previous reports [7, 24]. The FT-IR spectra of GS are shown in Fig. S1 as a supplementary file. The bands situated at about 2945.6, 1447.8, 1345.7, 1246.0, 1149.8, 1059.6, and 996.6 cm^{-1} in GS were shifted to 2855.8, 1735.0, 1459.9, 1206.7, 1136.5, 1094.1, and 982.9 cm^{-1} in MMT5-GS2 before calcination shown in Fig. 7c which confirms the existence of strong electrostatic interaction between GS and surface of catalyst in MMT5-GS2 before calcination [9].

From Fig. 7d, the absence of these peaks confirms that there is no surfactant remaining in the synthesized catalyst, MMT5-GS2 after calcination. This indicates that due to calcination at 450 °C, the surfactant is completely eliminated from nanocatalyst.

3.6. BET surface area analysis

To study the effect of bimetal doping and GS on the surface area and porosity nature of the as-synthesized TiO_2 nanoparticles of undoped TiO_2, MMT5 and MMT5-GS2, N_2 adsorption-desorption isotherms and their corresponding Berret-Johner-Halenda (BJH) pore size distribution plots were recorded and presented in Fig. S2a and S2b. From Fig. S2a, it results in a type -IV isotherm with H_2 hysteresis loop,

characteristic of the ordered mesoporous structure of the catalyst [25]. The average surface area, A_{BET} ($m^2 g^{-1}$) of all prepared catalysts was determined and tabulated in Table 2.

Table 2 Crystallite size, band gap energy and BET surface area of undoped TiO_2 and all bimetal doped and surfactant-assisted TiO_2 catalysts calcined at 450 °C

Serial number	Nanomaterials	Crystallite size (nm)	Bandgap energy (eV)	BET surface analysis		
				Surface area ($m^2 g^{-1}$)	Pore volume ($cm^3 g^{-1}$)	Pore size (nm)
1	Undoped TiO_2	18.30	3.20	64.1	0.22	10
2	MMT1	12.87	2.97	84.7	0.23	7.3
3	MMT2	12.05	2.83	83.7	0.22	7.2
4	MMT3	11.37	2.79	94.9	0.23	9.3
5	MMT4	11.74	2.75	91.4	0.24	8.1
6	MMT5	10.86	2.68	112.0	0.24	7.0
7	MMT5-GS1	10.22	2.76	140.6	0.24	7.3
8	MMT5-GS2	7.21	2.66	230.2	0.25	6.4
9	MMT5-GS3	8.33	2.83	160.1	0.22	8.3

From Table 2 the MMT5 has shown increased surface area (112 $m^2 g^{-1}$) compared to undoped TiO_2 (64 $m^2 g^{-1}$) due to crystal growth suppression by dopants. Whereas catalyst prepared in the presence of GS surfactant, MMT5-GS2 showed a higher surface area (230 $m^2 g^{-1}$) compared to both MMT5 and undoped TiO_2. It could be strong evidence for the decreased particle size of the TiO_2 resulting from the effective capping ability of the surfactant, which restricts the particle growth and nucleation during the synthesis process. To better compare the effect of bimetal doping and capping of GS on as-synthesized TiO_2 nanoparticles over single Mn^{2+} and Mg^{2+} doped TiO_2, comparative results are tabulated by referencing Mn [26] and Mg [27] single doped literature reports in Table 3.

Table 3 Comparative study of Mn^{2+}, Mg^{2+} single doped and Mn^{2+}/Mg^{2+} bimetal doped TiO_2 nanocatalysts

TiO_2 catalyst	Bandgap energy (eV)	Surface area ($m^2 g^{-1}$)	Crystallite size (nm)	References
Mn-TiO_2	2.98	93	21.8	[26]
Mg-TiO_2	2.92	49	20	[27]
Undoped TiO_2	3.2	64	18.3	Present work
MMT5	2.68	112	10.9	Present work
MMT5-GS2	2.66	230	7.2	Present work

3.7. PL Spectra

One of the essential reactive species in the process of photocatalysis is •OH which is responsible for oxidation reactions. Because of the high reactivity and short life of •OH, it is impossible for direct detection. To inspect the production of •OH from the catalyst during the photocatalysis reaction, a PL technique has been adopted using coumarin as a fluorescent probe molecule, which on reaction with •OH yields the 7-hydroxy coumarin [16]. In this technique, 0.1 g of catalyst is dispersed in 100 mL of 10 ppm coumarin solution in acidic conditions and illuminated to visible light irradiation. Small aliquots of reaction solution samples were withdrawn for every 30 min, filtered and PL intensity was measured in the range of 350-600 nm with excitation fixed at a wavelength of 435 nm. It has been observed from Fig. 8 that between 440-460 nm there exist PL spectra of the generating 7-hydroxy coumarin with maximum emission at 450 nm. A linear increase in PL intensity was observed with increasing irradiation time. However, in the absence of irradiation, no excitation was observed for the sample (0 min in Fig. 8).

From the above results, it could be understood that the number of •OH's produced on the catalyst surface was directly proportional to the irradiation time. The results further assure that the synthesized nanomaterial shows the enhanced rate of formation of •OH's under irradiation to visible light. This is due to the fact that the already formed photo holes in the valence band of bimetal doped TiO_2 could directly react with H_2O/OH^- to produce •OH [28].

4. Evaluation Of The Photocatalytic Activity Of Synthesized Mmt-gs Nanocatalysts By The Degradation Of Mr

Visible light assisted catalytic activity of the synthesized MMT-GS photocatalysts was evaluated by degradation of MR. For better photocatalytic degradation, the effect of reaction parameters like concentration of dopants, surfactant concentration, solution pH, catalyst dosage, and initial dye concentration was studied and optimized as follows.

4.1. Effect of metal ion dopant (Mn^{2+} and Mg^{2+}) concentration

In order to find out and optimize the best dopant concentration of bimetal doped photocatalyst among all the synthesized MMT photocatalysts, degradation experiments were carried out with each photocatalyst under visible light irradiation by taking catalyst dosage 0.05 g, solution pH 4, and initial MR concentration 10 mg L^{-1}. The rate of degradation of MR has been studied by measuring the MR absorbance, which is inserted in Fig. 9a. It can be seen from the figure that photocatalytic performance was found better for all the bimetal doped TiO_2 photocatalysts than undoped one and among all the synthesized photocatalysts, the best catalytic performance is shown by MMT5. This can be attributed to its narrowed bandgap resulting from the impurity energy levels between the valence band and conduction band that is created by the presence of both metal dopants which helps in the generation of more electron-hole pairs. Also, its small crystallite size and high surface area facilitate the adsorption of a greater number of dye molecules on its surface for degradation [7]. Therefore, based on the above results MMT5 was selected for optimizing other parameters.

4.2. Effect of GS concentration

To find out the optimal concentration of GS in MMT5 photocatalyst for efficient photocatalytic performance, as synthesized MMT5-GS catalysts with various wt% of GS (5, 10, and 15 wt%) along with MMT5 were tested by the degradation of MR under visible light irradiation by maintaining other parameters constant, i.e., catalyst dosage is 0.05 g, solution pH 4 and initial MR concentration 10 mg L^{-1}. It is observed from Fig. 9b that all MMT5 nanocatalysts prepared in the presence of GS degraded the MR in less time compared to MMT5 (Fig. 9a) which clearly indicates the significant role of the capping nature of the GS on the photocatalytic activity of MMT catalysts. From the apparent rate constants obtained by slopes of the individual curves (inset of Fig. 9b), it can be clearly seen that the degradation rate was increased up to 10 wt% GS concentration and then decreased on further loading. It could be due to the fact that increased GS concentration may restrict the effective doping of the metal ions into TiO_2 crystal lattice. Hence, MMT5-GS2 had been taken as a catalyst for further studies.

4.3. Effect of solution pH

According to Tang et al. [29], for charged substrates like TiO_2, there is a significant dependency on the pH value for the effective photocatalytic degradation, because the overall surface charge and adsorptive properties of TiO_2 nanomaterial depend strongly on solution pH. Hence, in this study, the effect of pH on the catalytic performance of the MMT5-GS2 was carried out by ranging the pH from 2 to 8 and keeping other parameters constant, i.e., catalyst dosage 0.1 g and initial MR concentration 10 mg L^{-1}. From Fig. 9c, it is observed that the degradation of MR is high in the acidic medium compared to the basic medium. This may be due to the strong electrostatic interaction between the positively charged surface (H^+ ions) of the catalyst and negatively charged dye molecules. When the pH increased to basic medium the catalyst surface acquires a negative charge and electrostatically repels the like-charged dye molecules. In specific, the degradation of MR is high at solution pH 4, because as the positive charge (H^+ ions) on TiO_2 surface increases, negatively charged MR can easily be adsorbed on the surface of the catalyst. And a further increase in pH greater than 4 will facilitate the hydrolysis of metal ions on the surface of TiO_2 which seizes its photocatalytic activity.

4.4. Effect of catalyst dosage:

To avoid the wastage of catalyst and minimize the screening effect, a number of experiments were carried out to get the optimum photocatalyst dosage by varying its amount ranging from 0.025 to 0.1 g using 10 mg L^{-1} of 100 mL of MR solution at solution pH 4. It was observed from Fig. 9d that the degradation of the MR increased linearly with the increase of catalyst loading up to 0.05 g because of the increased total surface area for dye adsorption. But after increasing the photocatalyst beyond 0.05 g, it creates turbidity and agglomeration of the catalyst particles due to excess photocatalyst and reduces the light transmission through the solution which leads to less photocatalytic activity [30]. And also, collisions between active molecules and ground-state molecules of bimetal doped TiO_2 results in the deactivation of the catalyst particles [16].

4.5. Effect of initial dye concentration

To study the effect of the initial dye concentration at a fixed weight of catalyst (0.05 g) and solution pH 4, the experiments were carried out with different concentrations of MR dye from 5 to 15 mg L^{-1} with results presented in Fig. 9e. The results demonstrate that the rate of degradation of MR dye increased up to 10 mg L^{-1}. But, a further increase in dye concentration causes the deactivation of the catalyst due to the blanket effect [31]. And because of the fixed catalyst dosage (0.05 g), there is no possibility to produce a sufficient number of •OH to counteract the increased number of dye molecules. Hence, the rate of degradation decreases.

5. Conclusions

GS abetted mesoporous Mn^{2+}/Mg^{2+} bimetal doped TiO_2 nanocatalysts were successfully synthesized by the sol-gel method without a change in the crystallinity of TiO_2 nanoparticles. The effective charge separation and narrowed band gap created by Mn^{2+}/Mg^{2+} bimetal ions doping and reduced particle size and increased surface area resulting from capping of GS had significantly enhanced the photocatalytic performance of MMT5-GS2 nanocatalyst towards the degradation of MR dye under visible light irradiation. The PL results exhibited that •OHs are the crucial reactive species responsible for oxidative photocatalytic degradation of MR. The highest degradation of MR was achieved in 60 min at optimized reaction conditions of 10 wt% GS on 0.25 wt% Mn^{2+}/1.00 wt% Mg^{2+} bimetal ions doped TiO_2, solution pH 4, catalyst loading of 0.05 g, and initial MR concentration 10 mg L^{-1}. Based on its effective photocatalytic activity, MMT5-GS2 nanocatalyst could be used as a promising material for the abatement of water pollution caused by organic dyes.

Declarations

Availability of data and materials

All data generated or analyzed during this study are included in this published article [and its supplementary information files].

Competing interests

The authors declare that they have no competing interests

Funding

Not Applicable

Authors' contributions

SRM planned the concept and carried out the experimental work. TSR supervised the research work and written the original draft. IMR interpreted characterization and experimental results, assisted in original draft writing and review & editing of the manuscript. SAA, GJ, and MLVPC were assisted in experimental work. All authors read and approved the final manuscript.

Acknowledgments

Not Applicable

References

1. Wang ZY, Chen C, Wu FQ, Zou B, Zhao M, Wang JX, et al. Photodegradation of rhodamine B under visible light by bimetal codoped TiO_2 J Hazard Mater. 2009;164:615–20.
2. Malika M, Rao CV, Das RK, Giri AS, Golder AK. Evaluation of bimetal doped TiO_2 in dye fragmentation and its comparison to mono-metal doped and bare catalysts. Appl Surf Sci. 2016;368:316–
3. Chelli VR, Golder AK. Bimetal doping on TiO_2 for photocatalytic water treatment: a green route. Eur Water. 2017;58:53–
4. Wang YQ, Zhang RR, Li JB, Li LL, Lin SW. First-principles study on transition metal-doped anatase TiO_2. Nanoscale Res Lett. 2014;9:46.
5. Divya Lakshmi KV, Siva Rao T, Swathi Padmaja J, Manga Raju I, Abdul Alim SK, Kalyani P. Visible light driven mesoporous Mn and S co-doped TiO_2 nano material: characterization and applications in photocatalytic degradation of indigo carmine dye and antibacterial activity. Environ Nanotechno Monit Manag. 2018;10:494–
6. Zhang CN, Chen SH, Mo L, Huang Y, Tian HJ, Hu LH, et al. Charge recombination and band-edge shift in the dye-sensitized Mg^{2+}-doped TiO_2solar cells. J Phys Chem C. 2011;115:16418–
7. Meshesha DS, Matangi RC, Tirukkovalluri SR, Bojja S. Synthesis, characterization and visible light photocatalytic activity of Mg^{2+} and Zr^{4+} co-doped TiO_2 nanomaterial for degradation of methylene blue. J Asian Ceram Soc. 2017;5:136–
8. Sofianou MV, Tassi M, Boukos N, Thanos S, Vaimakis T, Yu JG, et al. Solvothermal synthesis and photocatalytic performance of Mg^{2+}-doped anatase nanocrystals with exposed {001} facets. Catal Today. 2014;230:125–
9. Chekuri RD, Tirukkovalluri SR. Synthesis of cobalt doped titania nano material assisted by gemini surfactant: characterization and application in degradation of Acid Red under visible light irradiation. S Afr J Chem Eng. 2017;24:183–
10. Akpan UG, Hameed BH. The advancements in sol-gel method of doped-TiO_2 Appl Catal A-Gen. 2010;375:1–11.
11. Ikhmayies SJ. Characterization of nanomaterials. Jom-US. 2014;66:28–

12. Buitron G, Quezada M, Moreno G. Aerobic degradation of the azo dye acid red 151 in a sequencing batch biofilter. Bioresour Technol. 2004;92:143–
13. Lachheb H, Puzenat E, Houas A, Ksibi M, Elaloui E, Guillard C, et al. Photocatalytic degradation of various types of dyes (Alizarin S, Crocein Orange G, Methyl Red, Congo Red, Methylene Blue) in water by UV-irradiated titania. Appl Catal B-Environ. 2002;39:75–
14. Sahoo C, Gupta AK, Pal A. Photocatalytic degradation of Methyl Red dye in aqueous solutions under UV irradiation using Ag^{+} doped TiO_2. Desalination. 2005;181:91–
15. Divya Lakshmi KV, Siva Rao T, Swathi Padmaja J, Manga Raju I, Ravi Kumar M. Structure, photocatalytic and antibacterial activity study of Meso porous Ni and S co-doped TiO_2 nano material under visible light irradiation. Chin J Chem Eng. 2019;27:1630–
16. Raju IM, Rao TS, Lakshmi KVD, Chandra MR, Padmaja JS, Divya G. Poly 3-Thenoic acid sensitized, Copper doped anatase/brookite TiO_2 nanohybrids for enhanced photocatalytic degradation of an organophosphorus pesticide. J Environ Chem Eng. 2019;7:103211.
17. Shannon RD. Revised effective ionic radii and systematic studies of interatomic distances in halides and chalcogenides. Acta Crystallogr A. 1976;32:751–
18. Venkatachalam N, Palanichamy M, Murugesan V. Sol-gel preparation and characterization of alkaline earth metal doped nano TiO_2: efficient photocatalytic degradation of 4-chlorophenol. J Mol Catal A-Chem. 2007;273:177–
19. Jeong ED, Borse PH, Jang JS, Lee JS, Jung OS, Chang H, et al. Hydrothermal synthesis of Cr and Fe co-doped TiO_2 nanoparticle photocatalyst. J Ceram Process Res. 2008;9:250–
20. Padmaja JS, Rao TS, Lakshmi KVD, Raju IM. Fabrication of hetero-structured mesoporours TiO_2-$SrTiO_3$ nanocomposite in presence of Gemini surfactant: characterization and application in catalytic degradation of Acid Orange. J Environ Chem Eng. 2018;6:6457–
21. Ghobadi N. Band gap determination using absorption spectrum fitting procedure. Int Nano Lett. 2013;3:2.
22. Jaiswal R, Patel N, Kothari DC, Miotello A. Improved visible light photocatalytic activity of TiO_2 co-doped with Vanadium and Nitrogen. Appl Catal B-Environ. 2012;126:47–
23. Venkatachalam N, Palanichamy M, Arabindoo B, Murugesan V. Enhanced photocatalytic degradation of 4-chlorophenol by Zr^{4+} doped nano TiO_2. J Mol Catal A-Chem. 2007;266:158–
24. Sharotri N, Sharma D, Sud D. Experimental and theoretical investigations of Mn-N-co-doped TiO_2 photocatalyst for visible light induced degradation of organic pollutants. J Mater Res Technol. 2019;8:3995–
25. Deng QR, Gao Y, Xia XH, Chen RS, Wan L, Shoa G. V and Ga co-doping effect on optical absorption properties of TiO_2 thin films. J Phys Conf Ser. 2009;152:012073.
26. Lesnik M, Verhovsek D, Veronovski N, Gracner M, Drazic G, Soderznik KZ, et al. Hydrothermal synthesis of Mn-doped TiO_2 with a strongly suppressed photocatalytic activity. Mater Tehnol.

2018;52:411–
27. Behnajady MA, Alizade B, Modirshahla N. Synthesis of Mg-doped TiO_2 nanoparticles under different conditions and its photocatalytic activity. Photochem Photobiol. 2011;87:1308–
28. Mohamed MM, Al-Esaimi MM. Characterization, adsorption and photocatalytic activity of vanadium-doped TiO_2 and sulfated TiO_2 (rutile) catalysts: degradation of methylene blue dye. J Mol Catal A-Chem. 2006;255:53–
29. Tang WZ, An H. UV/ TiO_2 photocatalytic oxidation of commercial dyes in aqueous solutions. Chemosphere. 1995;31:4157–
30. Venkatachalam N, Palanichamy M, Murugesan V. Sol-gel preparation and characterization of alkaline earth metal doped nano TiO_2: efficient photocatalytic degradation of 4-chlorophenol. J Mol Catal A-Chem. 2007;273:177–
31. Subramani AK, Byrappa K, Ananda S, Rai KML, Ranganathaiah C, Yoshimura M. Photocatalytic degradation of indigo carmine dye using TiO_2 impregnated activated carbon. B Mater Sci. 2007;30:37–

Figures

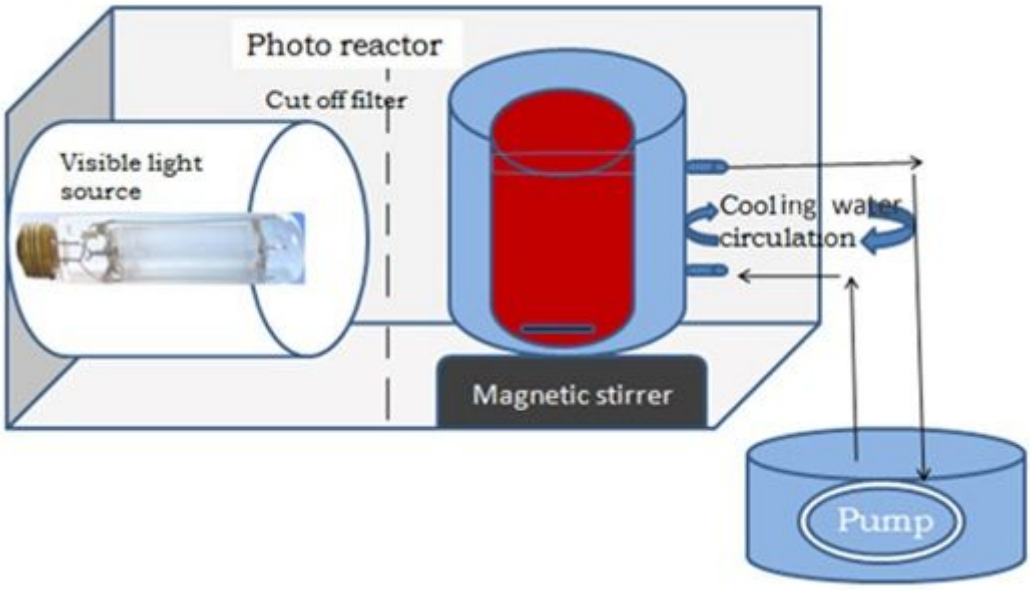

Figure 1

Schematic representation of photoreactor

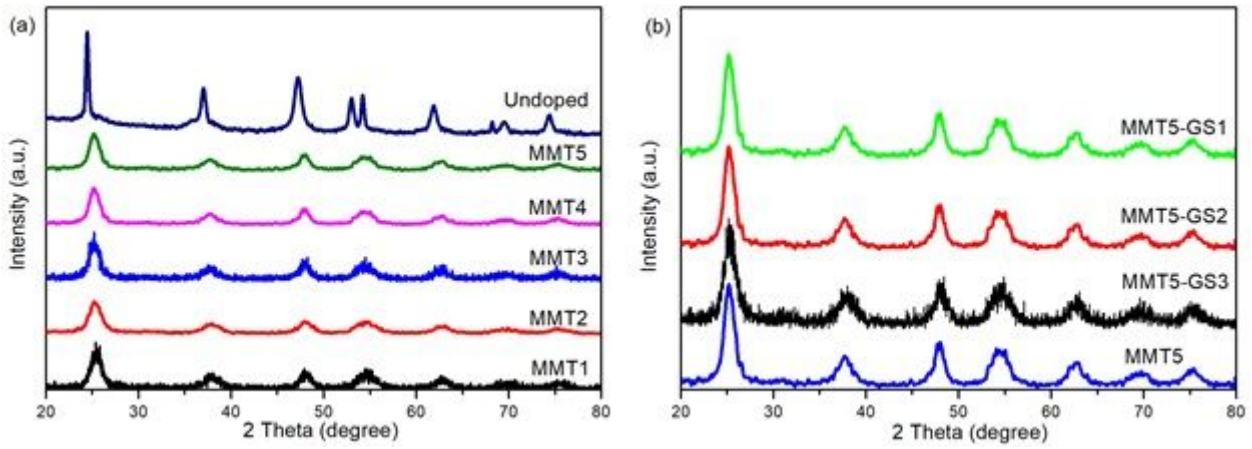

Figure 2

(a) XRD patterns of undoped TiO2 and Mn2+/Mg2+ bimetal doped TiO2 (MMT1-MMT5) catalysts, (b) MMT5 and surfactant assisted catalysts (MMT5-GS1- MMT5-GS3)

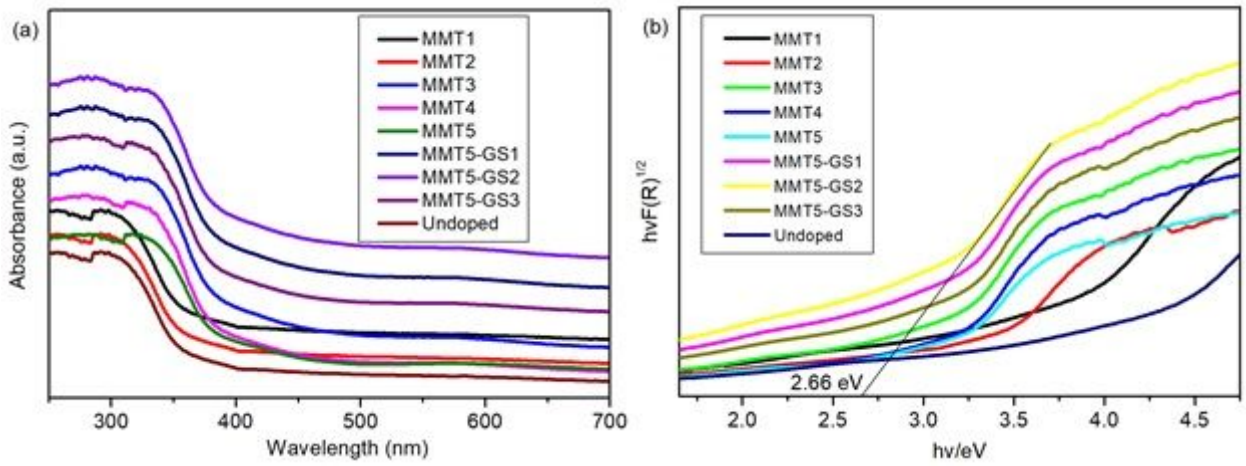

Figure 3

(a) UV-Vis DRS and (b) Kubelka-Munk formalism spectra of undoped TiO2, MMT and MMT5-GS catalysts

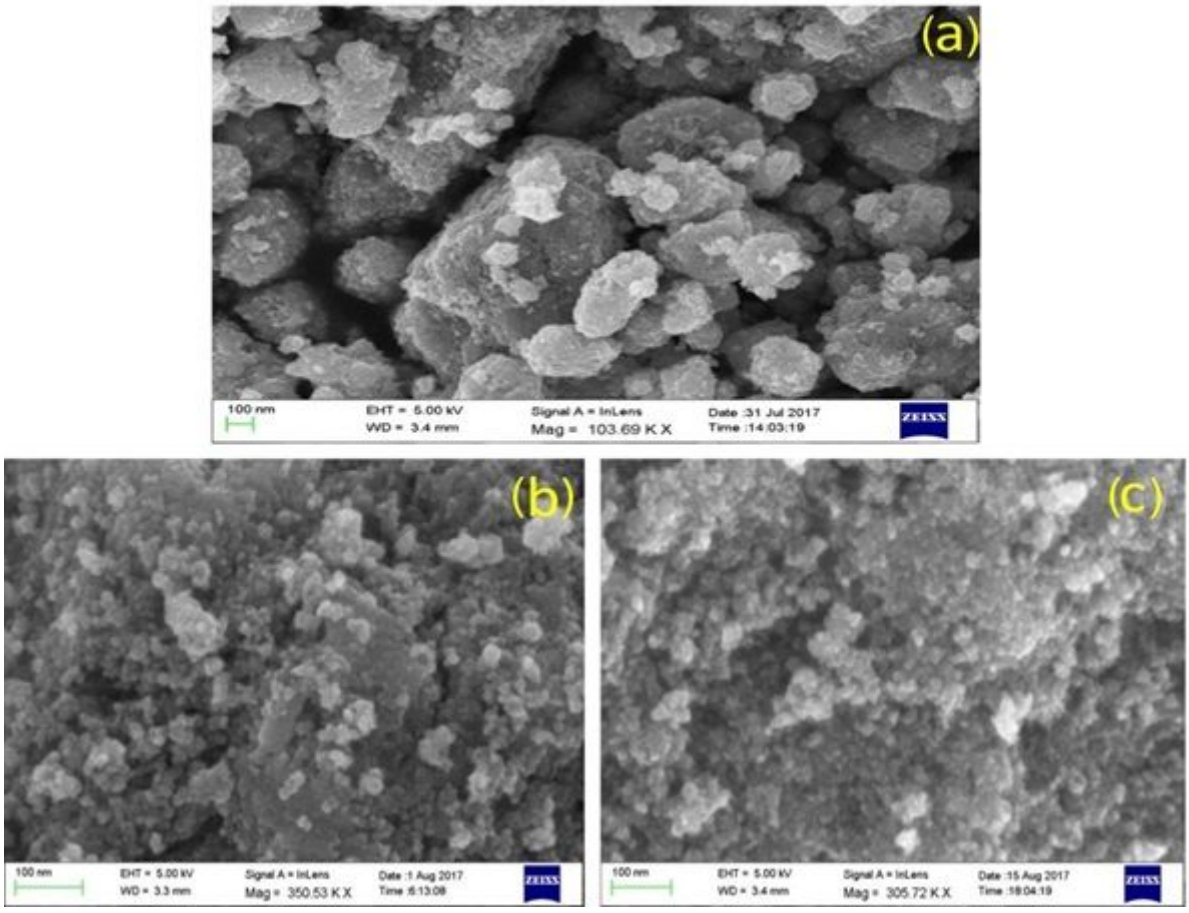

Figure 4

SEM micrographs of (a) Undoped TiO2, (b) MMT5 and (c) MMT5-GS2

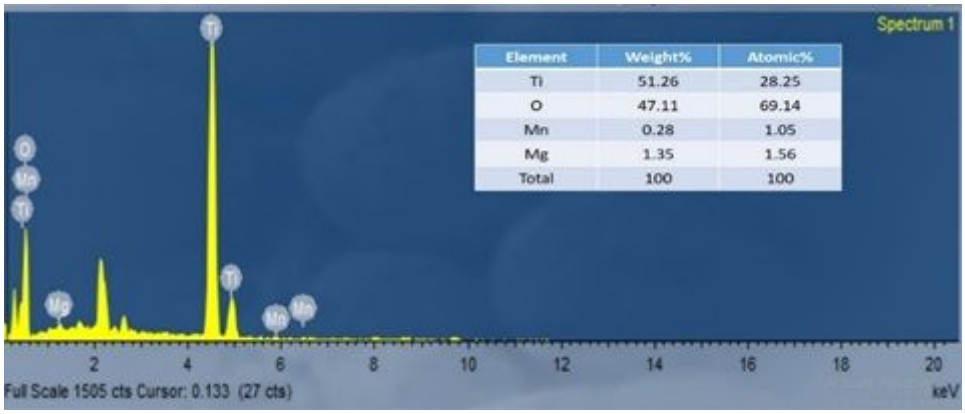

Figure 5

EDX spectrum of 0.25 wt% Mn2+ and 1.00 wt% Mg2+ bimetal doped TiO2 in the presence of 10 wt% of surfactant (MMT5-GS2) after calcination

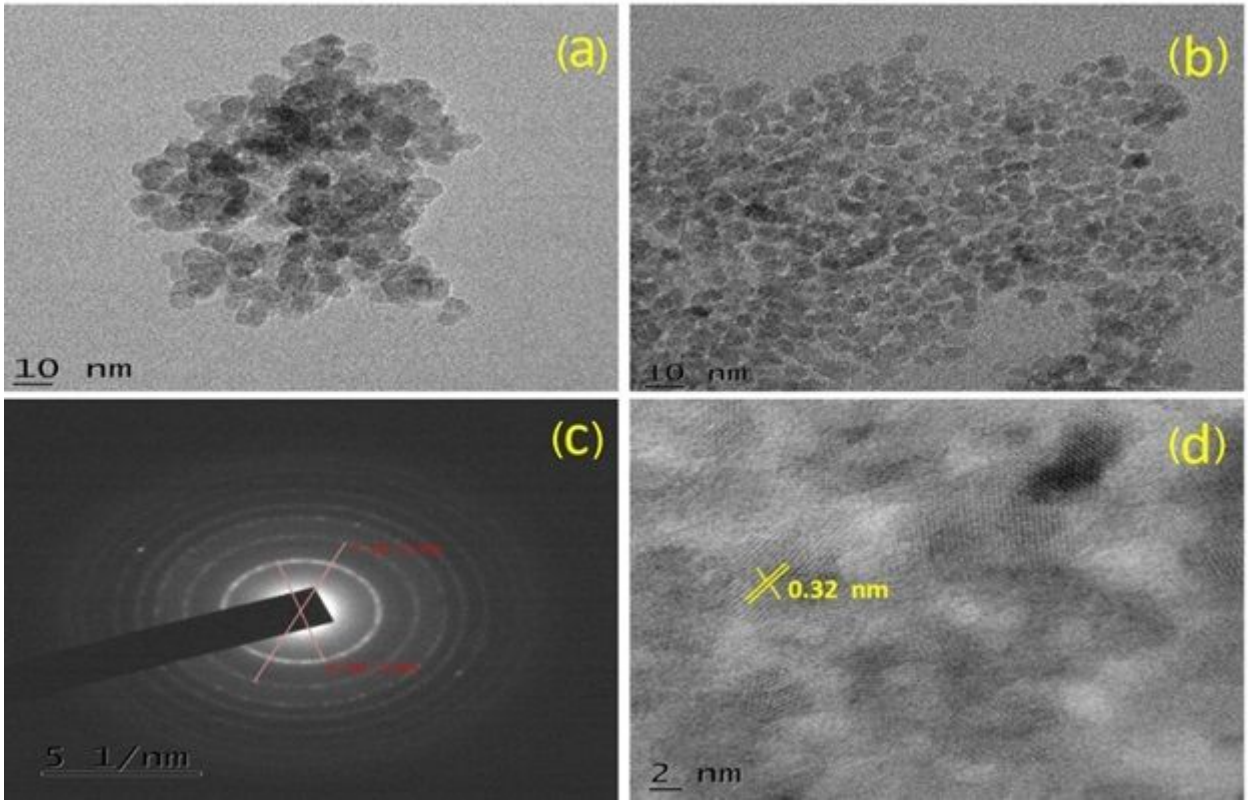

Figure 6

TEM image of (a) MMT5, (b) MMT5-GS2, (c) Selected area electron diffraction (SEAD) and (d) HRTEM image of MMT5-GS2

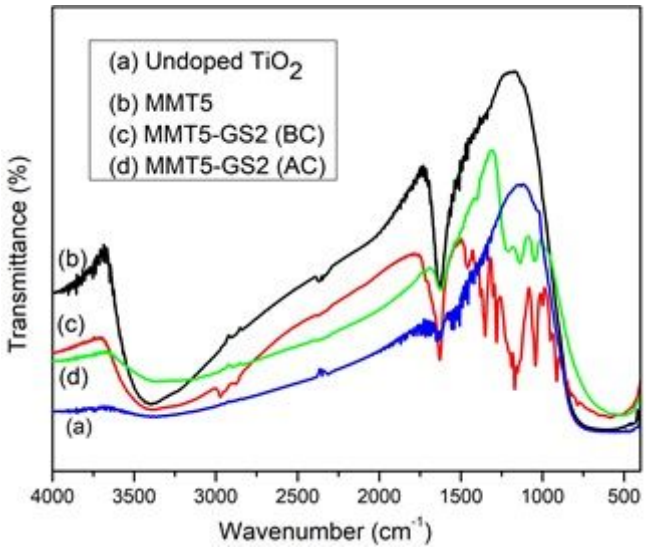

Figure 7

(a) FT-IR spectra of undoped TiO2, (b) MMT5, (c) MMT5-GS2 (before calcination), (d) FT-IR spectra of MMT5-GS2 (after calcination)

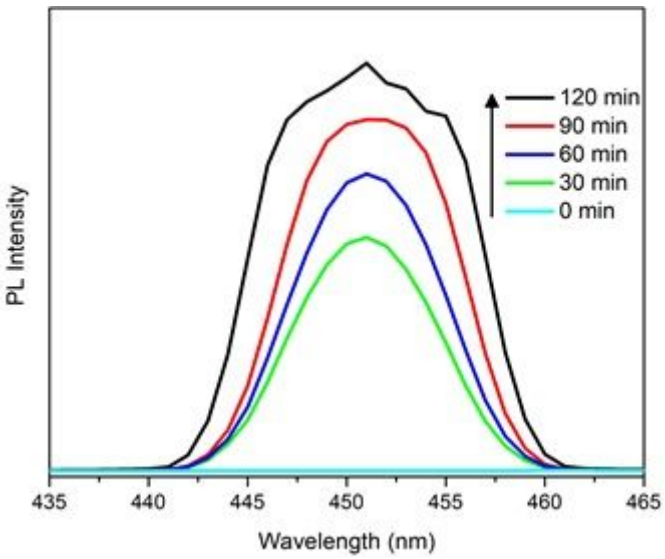

Figure 8

Photoluminescence spectra of MMT5-GS2

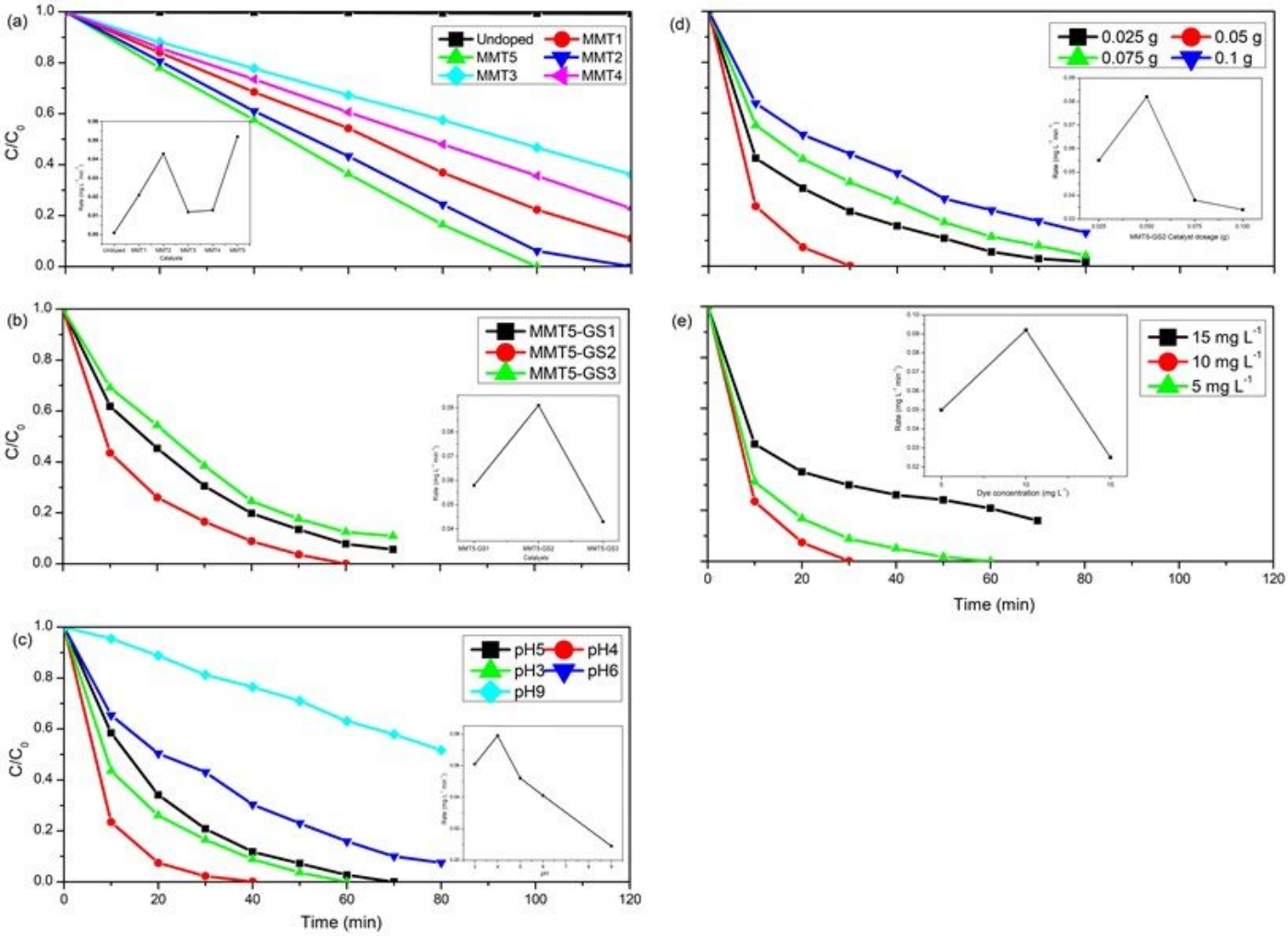

Figure 9

(a) Effect of dopant concentration of bimetal doped TiO2 on photocatalytic degradation of MR dye. Here, catalyst dosage 0.05 g, solution pH 4 and [MR]= 10 mg L-1. (b) Effect of GS concentration on the photocatalytic activity of MMT5 on the degradation of MR. Here catalyst dosage is 0.05 g, solution pH 4 and [MR] = 10 mg L-1. (c) Effect of pH on the rate of degradation of MR dye by MMT5-GS2. Here, catalyst dosage 0.1 g and [MR]=10 mg L-1. (d) Effect of catalyst dosage on the degradation of MR by MMT5-GS2. Here, solution pH 4 and [MR] =10 mg L-1. (e) Effect of the initial dye concentration on the rate of degradation of MR dye by MMT5-GS2. Here, solution pH 4 and catalyst dosage 0.05 g

Supplementary Files

This is a list of supplementary files associated with this preprint. Click to download.

- TypesettingSERED2000192Supplementarymaterials.pdf